A Piezo-Powered Floating-Gate Sensor Array for Long-Term Fatigue Monitoring in Biomechanical Implants

Nizar Lajnef, *Student Member, IEEE*, Niell G. Elvin, and Shantanu Chakrabartty, *Member, IEEE*

***Abstract*—Measurement of the cumulative loading statistics experienced by an implant is essential for prediction of long-term fatigue failure. However, the total power that can be harvested using typical in-vivo strain levels is less than 1 μW. In this paper, we present a novel method for long-term, battery-less fatigue monitoring by integrating piezoelectric transduction with hot-electron injection on a floating-gate transistor array. Measured results from a fabricated prototype in a 0.5-μm CMOS process demonstrate that the array can sense, compute, and store loading statistics for over 70 000 stress-strain cycles which can be extended to beyond 10^7 cycles. The measured response also shows excellent agreement with a theoretical model and the nominal power dissipation of the array has been measured to be less than 800 nW.**

***Index Terms*—Biomechanics, fatigue, piezoelectric transducers, self-powered sensing, strain sensors.**

I. Introduction

OVER THE last few decades, biomechanics has been at the forefront of biomedical research, primarily due to the success of arthroplasty, which refers to a surgical procedure to replace damaged joints and bones by prosthetic implants. Fig. 1 highlights some regions on a human skeletal system whose functionality can potentially be replaced by a biomechanical prosthetic implant. In 2003, approximately 600 000 hip and knee replacement surgeries were performed in the United States, and it is expected that the demand will grow by 174% for hip replacements and by 673% for knee replacements between 2005 and 2030 [1]. Typically, most of these prosthetic implants are expected to last for at least 20 years, after which patients require a revision and replacement surgery. However, a study by McGee [2] reported that wear and loosening of artificial joints leads to replacement of 10%–20% of implants within 15–20 years. It has also been reported that excessive wear of artificial knees leads to joint swelling (synovitis), bone loss (osteolysis), and, ultimately, fatigue due to misalignment or instability of the joint [3]. In many of these cases, revision surgery has proven to be more traumatic and less successful than the initial surgery. Therefore, monitoring these biomechanical implants for excessive wear and fatigue is essential for preventing premature failures and for significantly reducing patient discomfort and risk. Unfortunately, regular checkups may not be applicable to all patients due to the differences in their lifestyles and level of physical activity. An ideal solution is therefore to embed sensors and integrated circuits with the implant so as to monitor onset of fatigue before the occurrence of any catastrophic mechanical failure.

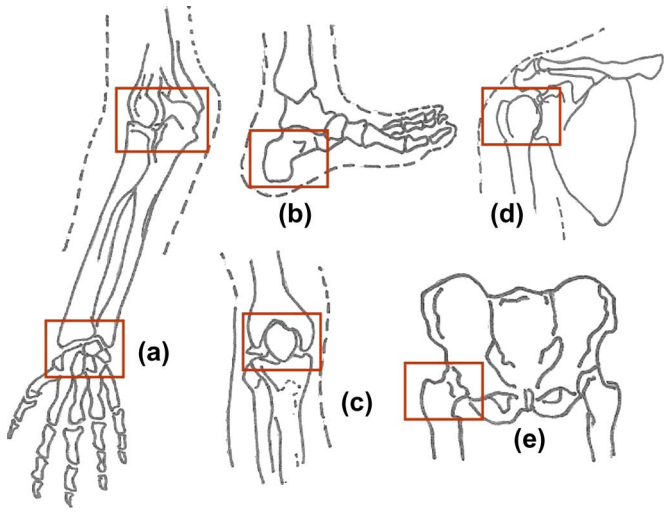

Fig. 1. Potential candidate regions for *in-vivo* monitoring of fatigue and wear. (a) Carpals. (b) Tarsals. (c) Patella/knee joints. (d) Scapula. (e) Scetabular (hip-socket) joint.

Previous studies have used implanted strain sensors for controlled monitoring of orthopedic implants. In [4], temporary implants containing four load cells were used to measure knee joint forces (a similar setup was also used to measure tibial forces). In [5]–[7], *in-vivo* strain gauges have been used in distal femoral replacements and in hip implants. However, in most of these experiments, the focus has been for logging data only for short durations, and power is typically derived through inductive or ultrasonic coupling or through external leads in skin. Unfortunately, both powering methods limit the mobility of the patient and therefore are unrealistic for long-term autonomous monitoring.

Manuscript received November 01, 2007; revised February 26, 2008. Current version published October 24, 2008. This work was supported by the National Science Foundation under Grant CMMI: 0700632. This paper was recommended by Associate Editor Y. Lian.

N. Lajnef is with the Department of Civil and Environmental Engineering, Michigan State University, East Lansing, MI 48824 USA (e-mail: lajnefni@egr.msu.edu).

N. G. Elvin is with the Department of Mechanical Engineering, Columbia University, New York, NY 10026–6902 USA (e-mail: elvin@egr.msu.edu).

S. Chakrabartty is with the Department of Electrical and Computer Engineering, Michigan State University, East Lansing, MI 48824 USA (e-mail: shantanu@egr.msu.edu).

Color versions of one or more of the figures in this paper are available at http://ieeexplore.ieee.org.

Digital Object Identifier 10.1109/TBCAS.2008.2001473

TABLE I
TYPICAL STRAIN LEVELS IN *IN-VIVO* BIOMECHANICAL STRUCTURES

Structures	Typical Strain levels
Nerves	0.1% - 20% [19]
Bones	0.04% - 0.16 % [20]
Ligaments	0.1% - 4 % [21]
Muscles	0.1% - 5 % [22]

One of the attractive solutions towards achieving autonomy in long-term monitoring is "self-powered sensing," where electrical energy is harvested directly from the signal being sensed. In this regard, piezoelectric transducers provide an adequate mechanism for sensing fatigue in an implant and for self-powering of the sensors through energy harvesting [8]. In [9], a micro-implant was proposed that is capable of generating 1 mW of power from stretching of human ribs during breathing. In [10], a piezoelectric implantable internal fracture fixation device was described that was capable of generating microampere current either through external ultrasonic actuation or through direct loading during walking. Piezoelectric implants have also been proposed in the area of orthopaedics [10]–[13], dentistry [13], audiology [14], cardiology [15], and neurology [16].

Two different piezoelectric material classes are commonly used for electric energy harvesting. The first class of material is a ceramic composed of lead zirconate titanate (PZT), and the second is a semi-crystalline plastic polyvinylidene fluoride (PVDF). PVDF has been extensively used in medical sutures due to its excellent flexibility and biocompatibility [17]. The biocompatibility of PZT is unknown. However, since one of the basic elements of PZT is lead, it is unlikely that it will be readily implanted without significant testing and approval by the Food and Drug Administration (FDA). Furthermore, the brittleness of PZT could cause particular debris which might be toxic to cells. A major disadvantage of PVDF is its very low mechano-electrical energy conversion. Given the typical strain levels experienced by biomechanical structures (Table I) and using a piezo-generator model, the extractable power was estimated to be less than 1 μW for a PVDF sheet of dimensions "31 mm $\times$ 16 mm $\times$ 0.028 mm" loaded at a 1-Hz frequency. We have also shown experimentally that the power generated from a PVDF sensor for a hip implant (Fig. 2) under physiological load is indeed 1 μW [11]. This is well below the 50 mW that is currently required for commercially available ultralow-power wireless sensor nodes (TelosMote) and is also less than the 1-mW power level reported by Arms *et al.* [18]. These sensors still require 100 times more power than what would be available under normal physiological conditions. In addition to ultralow power levels, the occurrence of loading cycles is infrequent necessitating integration of self-powered computation and sensing with nonvolatile storage.

One of the attractive properties of piezoelectric transducers is its ability to generate large voltage swings (>5 V), but at nanoamperes current level. This property is ideal for triggering avalanche injection in floating-gate transistors and in [26], we demonstrated its feasibility to achieve sensing, computation and storage at power levels less than 1 μW. In this paper we extend the work in [26] by presenting a detailed mathematical model and a calibration procedure for the piezo-powered floating gate injector array. The paper is organized as follows: Section II briefly presents an overview of a commonly used fatigue prediction algorithm. Section III describes the principle of operation of a floating-gate injector circuit and presents a mathematical model describing its behavior. Section IV describes a circuit implementation of the floating-gate injector array. Section V presents measurement results obtained from a fabricated prototype Section VI concludes with some final remarks and discussions.

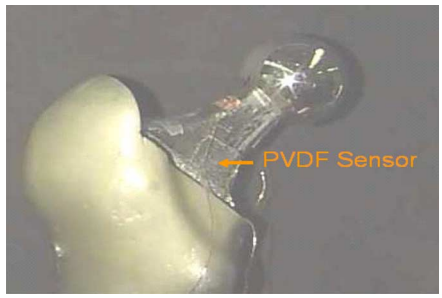

Fig. 2. Stainless steel hip implant reported by the authors in [11] showing PVDF sensor/generator attached for monitoring torsional loading.

II. FATIGUE AND FATIGUE PREDICTION

Mechanical fatigue is the accumulation of damage in a structure under applied fluctuating stresses. Even though the magnitudes of the applied stresses could be less than the tensile strength of the material, the progressive fatigue damage may ultimately lead to complete mechanical failure. Fatigue life is defined as the number of load cycles necessary to induce failure and is a function of the level of fluctuating stress/strain in the structure. This is typically expressed using an S-N curve [24] which is used for determining the life of a structural component under constant amplitude low stress levels (within the elastic limit of the material). An example of an S-N curve is shown in Fig. 3(a). Higher strain levels require fewer cycles to cause damage, whereas low-strain levels which are typical in most orthopedic implants require many more cycles to cause damage. An important consequence of the S-N curve is that stress cycles less than the so-called "fatigue limit" stress should not cause the material to fail (often taken as a stress level that can withstand 10^7 cycles). The fatigue sensor could therefore ignore input signals below a level that is calibrated to match the fatigue limit of the implant. However, the S-N curve can not be directly used to determine the fatigue in an implant, as in real-world conditions, the magnitude of the applied cyclic loads vary depending on the environmental conditions. For example, walking, running, or climbing can produce significantly different loading conditions in a knee or hip implant. Several algorithms have therefore been devised for fatigue lifetime predictions under nonperiodic loading conditions. The most common and widely used algorithm is the Palmgren–Miner's Rule [24], often simply called the Miner's rule. In its basic form, the Miner's rule assumes that each strain cycle with quantized magnitude ε_i consumes $1/N_i$

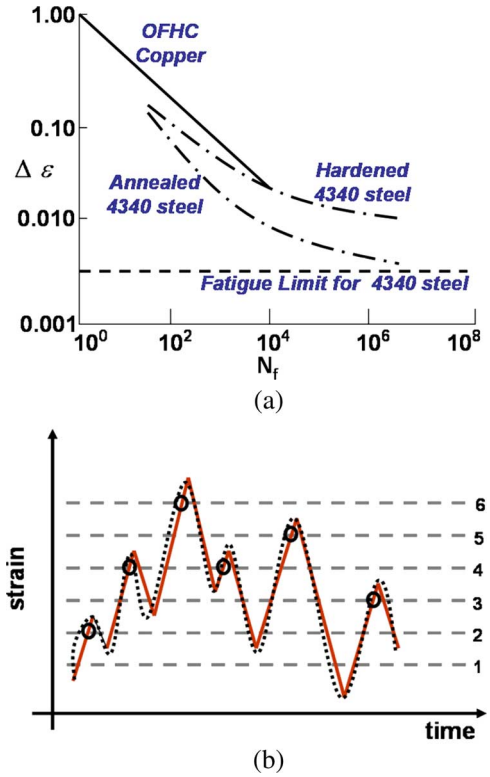

Fig. 3. (a) An example of an S-N curve (redrawn with parameters adapted from [25]). (b) Illustration of the Miner's rule applied to a recorded strain waveform.

of the total fatigue life, where N_i is the number of fatigue cycles taken to fail the material at that strain level. Algebraically, this can be stated as

$$\sum_{i=1}^{P} \frac{n_i}{N_i} = 1. \tag{1}$$

To apply Miner's rule, the recorded strain levels are quantized into different threshold ε_{i}, $\mathrm{i} = 1, \ldots, \mathrm{P}$, as shown in Fig. 3(b). The algorithm then counts the total number of occurrences when the magnitude of strain exceeds each of the threshold ε_{i} [denoted by circles in Fig. 3(b)]. The total count of events denoted by n_i is then normalized by N_i (from the S-N curve) according to (1). The underlying principle behind the proposed sensor is to compute the features n_i which can then be used in Miner's rule for prognosticating fatigue in an implant.

III. Principle of Operation and Electrical Model

A simplified schematic of the proposed sensor that can compute parameters n_i in (1) is shown in Fig. 4. It consists of a p-channel floating-gate metal–oxide–semiconductor (MOS) transistor which is connected to a piezoelectric transducer.

The vibration energy harvested by the piezoelectric transducer is used to inject electrons from the transistor channel onto the floating-gate $\mathrm{V_g}$. Injection of electrons in a pMOS transistor is based on an ionized hot-electron injection (IHEI) process which occurs when a high electric field is formed at the drain-to-channel depletion region. The high-electric field in the depletion region creates hot-electrons due to impact ionization. The

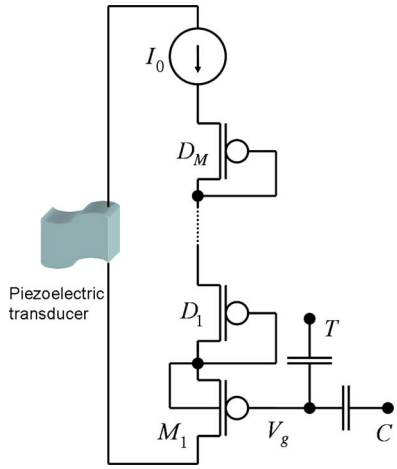

Fig. 4. Simplified circuit model for piezo-driven floating-gate sensor.

released electrons travel back into the channel region, gaining energy, and, when their kinetic energy exceeds the silicon and silicon-dioxide barrier (>3.2 eV), the electrons are injected into the oxide. As more electrons are added to the floating-gate transistor, its potential decreases, which results in an equivalent increase in the drain current through the transistor.

Since the floating-gate transistor, is surrounded by high-quality insulation, any electrical charge injected onto this gate is retained for long time (loss of 1% over a period of eight years) [29]. Hot-electron injection in a pMOS transistor is a feedback process because an increase in injection onto the floating gate (decrease in gate potential) reinforces the injection process. However, the injection rate of the floating-gate transistor M1 can be controlled by limiting the source current to a constant current reference $\mathrm{I_0}$, as shown in Fig. 4. Even though several empirical formulations exist for modeling IHEI in terms of gate, drain, and source voltages, we have found the following expression for $\mathrm{I_{inj}}$ to be sufficient:

$$I_{\mathrm{inj}} = \beta I_0 e^{V_{\mathrm{sd}}/V_{\mathrm{inj}}} \tag{2}$$

where V_{sd} is the drain-to-source voltage and I_0 is the source current. For a pMOS transistor fabricated in a standard 0.500μm CMOS process and biased in weak-inversion, a drain-to-source voltage greater than 4.2 V has been found to be sufficient for triggering any observable effects of the IHEI process. The charge on the floating-gate transistor can also be modified using Fowler–Nordheim (FN) tunneling [26], where the electrons are removed by applying a high voltage (>14 V in a 0.5-μm CMOS process) across the tunneling capacitor T.

A. Mathematical Model of the Floating-Gate Injector

In weak inversion, the expression for source current through the pMOS transistor M1 is given by

$$I_0 = I_s e^{-\kappa \frac{V_g}{U_T}} e^{\frac{V_s}{U_T}} \tag{3}$$

where I_0 is the source current, I_s is a pre-exponential current, V_g is the floating-gate voltage, κ is the floating-gate efficiency, and U_t is the thermal voltage (26 mV at room temperature). For

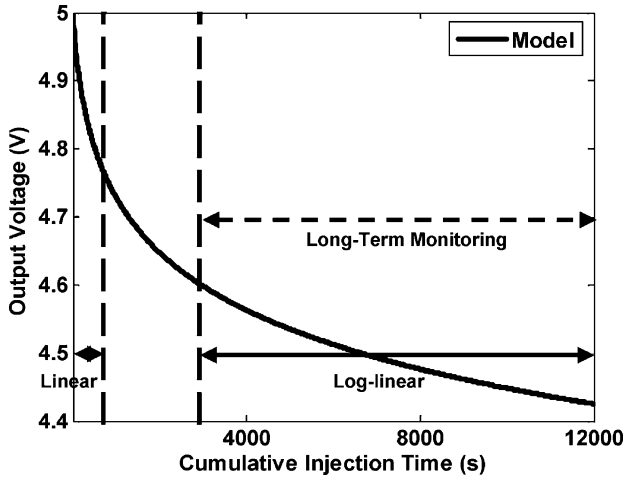

Fig. 5. Output of the floating-gate injector based on the mathematical model given by (6).

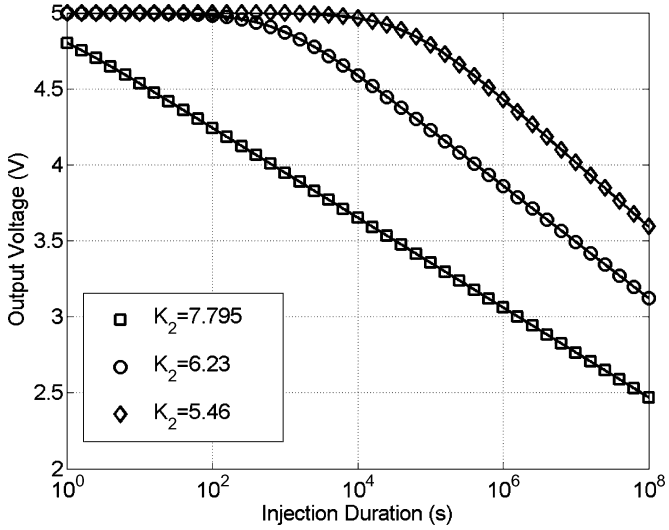

Fig. 6. Response of the floating-gate injector for different values of K_2.

the fixed reference current I_0, the gate current of M1 according to the IHEI model (2) is given by

$$I_g = \beta I_0 e^{V_s/V_{\text{inj}}} = -C_t \frac{\partial V_g}{\partial t} \tag{4}$$

where β and V_{inj} are constants and C_t is the total capacitance of the floating node V_g. Combining (3) and (4) gives the following differential equation for V_g:

$$\frac{\partial V_g(t)}{\partial t} = -K_1 e^{K_2 V_g(t)} \tag{5}$$

with

$$K_1 = \left(\frac{\beta I_0}{C_t}\right)\left(\frac{I_0}{I_s}\right)^{\frac{U_T}{V_{\text{inj}}}}$$
$$K_2 = \frac{\kappa}{V_{\text{inj}}}.$$

The solution of (5) gives the change in floating-gate voltage V_g with respect to time t and transistor drain current I_o as

$$V_g(t) = -\frac{1}{K_2}\log\left(K_1 K_2 \int\limits_{\tau \in t} \partial\tau + e^{-K_2 V_{g0}}\right) \tag{6}$$

where V_{g0} is the initial gate voltage and t in (6) represents the total duration for which the injector is operational.

The output voltage $V_s(t)$ can be expressed in terms of $V_g(t)$ as

$$V_s(t) = V_g(t) + K_3 \tag{7}$$

where

$$K_3 = U_T \log(I_0/I_S).$$

Fig. 5 shows a typical response of the output voltage $V_{out}(t)$ as a function of injection duration t. The response as shown in Fig. 5 consists of two distinct regions.

The linear region which is characterized by the condition $t \ll (\exp(-K_2 V_{g0})/K_1 K_2)$. In this region, (6) can be simplified to

$$V_{\text{out}}(t) = V_{g0} + K_3 - \frac{K_1 K_2}{\exp(-K_2 V_{g0})} t \tag{8}$$

where the approximation $\log(1+x) \approx x$ has been used. Thus, in the linear region, the change in the output voltage is linear with respect to the injection duration and therefore is suitable for short-term fatigue monitoring (typically less than 100 loading cycles). The other region, which is important for long-term fatigue monitoring, is the log-linear region and is characterized by the condition $t \gg (\exp(-K_2 V_{g0})/K_1 K_2)$, which, when applied to (6), leads to

$$V_{\text{out}}(t) = K_3 - \frac{1}{K_2}\log(K_1 K_2) - \frac{1}{K_2}\log(t). \tag{9}$$

Thus, the change in output voltage is a logarithmic function of time and therefore can be used for long-term event monitoring. The first part in (9) is an offset term which captures the dependence of the output voltage on the biasing conditions, initial conditions, and ambient temperature. Figs. 6 and 7 show the output voltage $V_s(t)$ plotted on a logarithmic scale for typical values of parameters K_1, K_2. It can be seen from Fig. 6 that the slope of the log-linear response is a function of K_2 and, hence, can be used to extend the monitoring duration of the sensor. Using typical parameters obtained from a 0.5-μm CMOS process, we have verified that "log-linear" response can easily last beyond a million injection seconds. As shown in Fig. 7, the process-dependent parameter K_1 only introduces an offset in the log-linear response. This will be important for compensating the response of the injector for initialization errors and can be seen when (9) is expressed in its incremental form as

$$\Delta V_S(t) = -\frac{1}{K_2}\log\left(\frac{t}{t_0}\right). \tag{10}$$

where $\Delta V_S(t)$ is the change in voltage measured with respect to the voltage at a reference time-instant t_0.

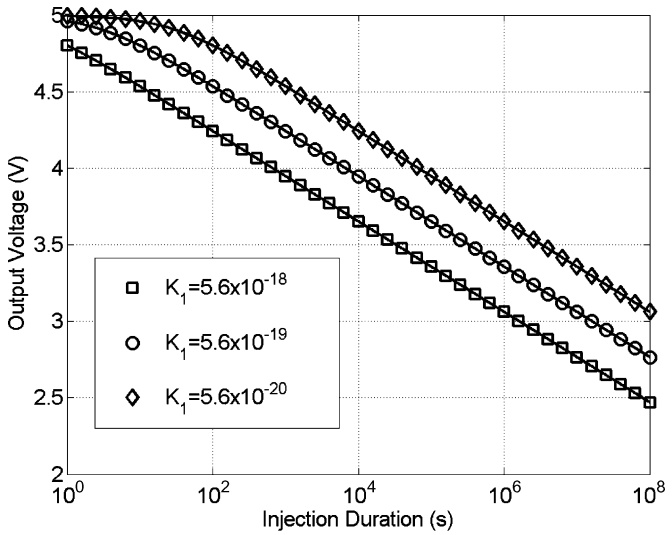

Fig. 7. Response of the floating-gate injector for different values of K_1.

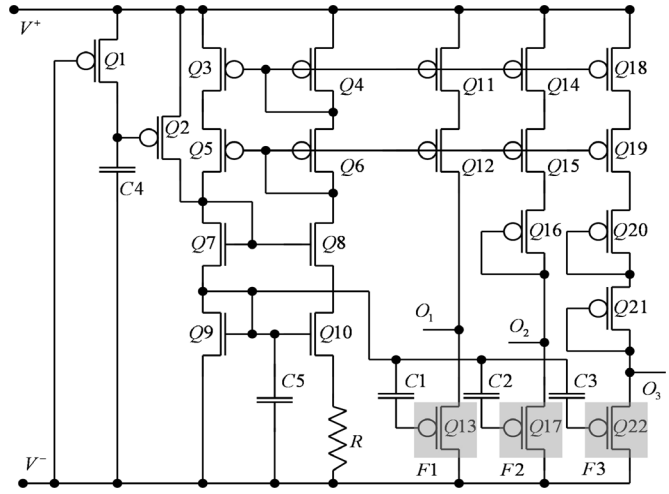

Fig. 8. Circuit implementation of the floating-gate reference array.

B. Event Detection

Diodes $\mathrm{D}_1 - \mathrm{D}_\mathrm{M}$ in Fig. 4 control the potential drop between the supply terminal and the source of the floating-gate transistor. The placement of a different number of diodes ensures that the floating-gate injector is operational at different voltages generated by the piezoelectric transducer. For an injector circuit consisting of M diodes between the current source and the floating-gate transistor, the minimum supply voltage required for onset of injection is

$$V_{\mathrm{dd}} = 2V_{\mathrm{dsat}} + MU_T \log\left(\frac{I_0}{I_d}\right) + V_{s0} \tag{11}$$

where $2V_{\mathrm{dsat}}$ is the drain-to-source voltage drop for a cascaded current source, I_d is pre-exponential current for the pMOS diode transistors, and V_{s0} is the initial floating-gate source voltage. For transistors biased in weak inversion $V_{\mathrm{dsat}} \geq 3U_T$, we have

$$V_{\mathrm{dd}} \geq 6U_T + MU_T \log\left(\frac{I_0}{I_d}\right) + V_{s0}. \tag{12}$$

For $V_{S0} = 5$ V, the inequality (12) leads to

$$V_{\mathrm{dd}} \geq 0.6M + 5.15. \tag{13}$$

Therefore, the piezoelectric transducer has to generate a voltage pulse with minimum amplitude of 5.15 V. While interfacing the transducer with the floating gate sensor array, this minimum supply voltage should be set to be equal to the piezoelectric voltage output representing the fatigue limit of the material [see Fig. 3(a)].

IV. Circuit Implementation

A circuit implementation of an array of floating-gate injectors with an integrated current reference is shown in Fig. 8 and Table II. The reference current generator circuit is implemented using transistors Q1–Q10 and resistor R. As in a standard current reference circuit, the ratio of the pMOS current mirror transistors Q3 and Q4, denoted by K, determines the magnitude of the reference current and is given by

$$I_0 = U_T \log(K)/R. \tag{14}$$

Transistors Q1 and Q2 form a start-up circuit for the current reference. The reference current is copied by mirrors Q11, Q14, and Q18, which drive the floating0gate cells F1–F3. Diode-connected transistors Q16, Q20, and Q21 are used to control the potential drop between the supply terminal and source of the floating-gate transistors Q13, Q17, and Q22, which ensures that each of the floating-gate cells (F1–F3) start injecting at different supply potential $(V^+ - V^-)$. When a potential is applied across the supply terminals (V^+, V^-), the circuit generates both a reference current and a stable voltage reference used for biasing the floating-gate transistors. Depending on the magnitude of the rectified voltage, different cells F1–F3 will start injecting electrons into their floating gate. The array directly interfaces with a piezoelectric transducer through a full-wave rectifier, implemented using a standard diode bridge. For the prototype presented in this section an n^+-p substrate and p^+-n well diodes were used, which are naturally integrated on an electrostatic discharge (ESD) protection pads of the VLSI chip. A storage capacitor is used at the output of the rectifier to filter out unwanted high-frequency components. The size of this capacitor also provides a tradeoff between the total hold-time versus the voltage swing at the sensor.

TABLE II
Transistor, Resistor, and Capacitor Sizes Used for Implementing the Reference Array

Element	Size
Q4,Q5,Q6,Q11,Q12,Q14, Q15,Q18,Q19	30μm/10μm
Q16,Q20,Q21	10μm/10μm
Q13,Q17,Q22	6μm/6μm
Q1,Q2.Q3	60μm/10μm
Q7,Q8,Q9,Q10	60μm/10μm
C4,C5	1pF
R	1.5MΩ

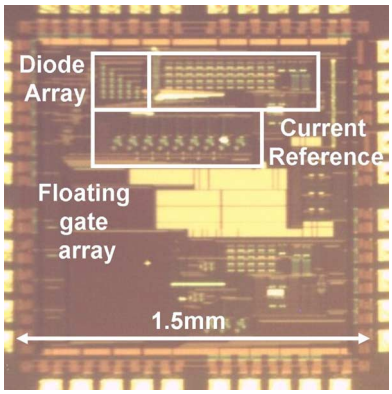

Fig. 9. Micrograph of the prototype floating-gate sensor.

TABLE III
SUMMARY OF SPECIFICATIONS MEASURED USING THE FABRICATED PROTOTYPE

Parameter	Value
Technology	0.5 μm CMOS
Size	1.5mm x 1.5mm
Number of Injectors	7
Injection Range	4.2V-8V
Maximum Current	160nA
Startup Time	<30ms

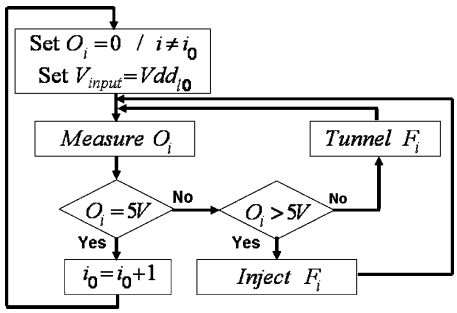

Fig. 10. Flowchart describing the sensor initialization algorithm.

V. EXPERIMENTAL AND MEASUREMENT RESULTS

A prototype floating-gate injector array has been fabricated in a standard 0.5-μm CMOS process (micrograph is shown in Fig. 9) and its specifications are summarized in Table III.

Before the prototype can be used for continuous monitoring, an equalization procedure is required to initialize the charge stored on the gate of the floating-gate injectors. Fig. 10 shows a flowchart that summarizes the equalization procedure. Initially, each of the floating-gate cells (F1–F3) is programmed (using tunneling and injection) to a fixed floating-gate voltage. The gate voltages are indirectly monitored by measuring the output voltages of each of the floating-gate cells ($O_{\rm i}$, $i = 1, 2, \ldots, 7$). For different supply voltages ($\rm Vdd_i$, $i = 1, 2, \ldots, 7$), the cells F1–F7 were programmed until the output voltage $V_{\rm oi}$ is set to a fixed potential (5 V for this work).

After equalization, the prototype was connected to a programmable signal generator which was used to simulate the output of a piezoelectric transducer. In this experiment, pulses with three different voltage levels were chosen, where each of the levels trigger different floating gate injectors. The startup time for the current reference and injection circuitry was measured to be less than 30 ms, which is sufficient for a typical loading cycle (1000 ms). Fig. 11(a)–(c) showsthe measured output voltages $O_1 - O_3$ corresponding to the three injector cells F1–F3 for voltage pulses of different amplitudes ($\rm Vdd_1 = 5.3$ V, $\rm Vdd_2 = 6.1$ V, and $\rm Vdd_3 = 6.9$ V).

It can be seen from Fig. 11(a) that only cell F1 injects when pulses of amplitude of 5.3 V are applied. Also, the response of the injector F1 is a log-linear function of the injection duration. Cells F2 and F3, on the other hand, show negligible injection compared with cell F1. Fig. 11(b) shows the response of the injector array when voltage pulses with amplitude of 6.1 V were applied. Both F1 and F2 inject at an identical rate, whereas cell F3 shows negligible injection. Thus, cells F1 and F2 count the duration of the event when the input voltage exceeds 6.1 V. For pulses with amplitude greater than 6.9 V, all the cells F1–F3 inject at an identical rate, and the response in Fig. 11(c) show excellent agreement with the mathematical model in (6). Using the model in (6), it can be calculated that the duration of injection before the output voltage approaches the injection threshold (4.2 V) is approximately 70 000 s. This period can only be increased beyond 10^8 s by decreasing the parameter K_2, as was shown in Fig. 6.

The second set of experiments was designed to evaluate the performance of the injector array under variable loading conditions. The floating-gate injectors were first equalized using the algorithm as described in Fig. 10. The programmable voltage source was then used to generate three periodic waveforms, each consisting of three voltage levels (5.3, 6.1, and 6.9 V). The duration of the voltage levels, as shown in Fig. 12(b) and (c), was chosen in a predefined proportion. For instance, the waveform used for one of the experiments is shown in Fig. 12(b); the duration of the three levels were in the proportion of 3:2:1. The corresponding response measured from the injector array is shown by the solid line in Fig. 12(a). The difference in the injection duration translates into an offset in the log-linear response, and this is evident from the measured results. Fig. 12(a) also shows the measured response (dotted line) of the injector array corresponding to the input waveform in Fig. 12(c). The response of injector F1 remains unchanged, whereas the response corresponding to injector F3 demonstrates an increased offset relative to the response of F1, which is consistent with the decrease in duration of 6.9-V pulses in Fig. 12(b). On the other hand, the response of injector F2 shows a reduced offset due to increase in duration of 6.1-V pulses. It can be seen from the measured results that the injector array indeed captures the statistics of cyclic loads as the duration of voltage levels is varied.

For the last set of experiments, the prototype injector array was interfaced with a piezoelectric transducer (PZT). The transducer was mounted on an extruded acrylic cantilevered beam. The beam was then subjected to periodic loading cycles. An external capacitor (100 nF) was chosen which is equivalent to voltage swing of up to 8 V across the rectifier when a 20-V pulse is generated by the PZT. An over-voltage protection and clamping circuitry (consisting of zener diodes) was integrated at the output of the diode bridge to prevent damage due to unwanted piezoelectric surges. Fig. 13(a) shows a sample waveform recorded at the output of the half-wave rectifier integrated on-chip with the injector array showing that, for the loading

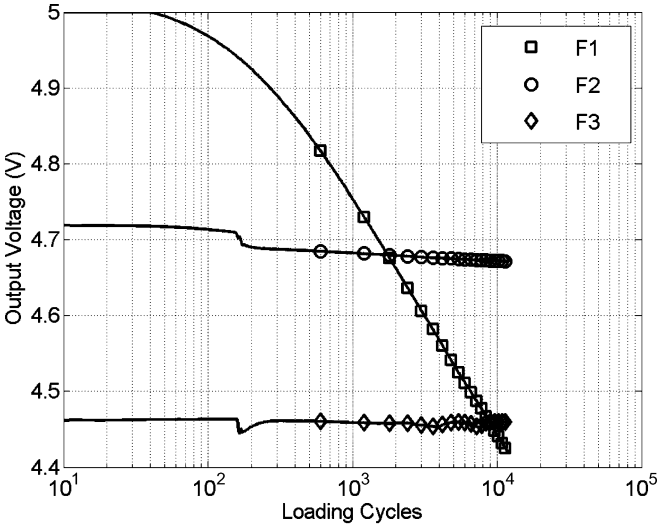

(a)

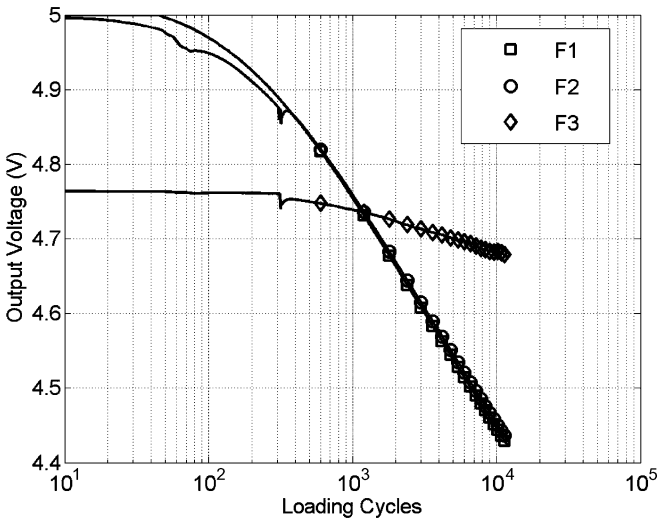

(b)

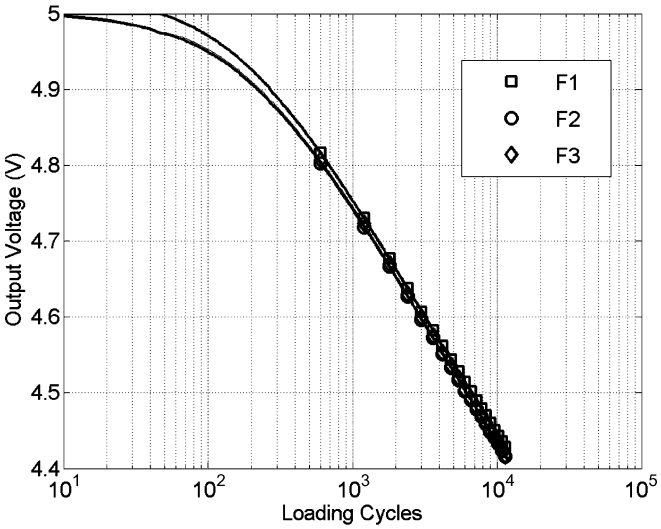

(c)

Fig. 11. Measured source-to-drain voltage response across the floating-gate elements at $\mathrm{Vdd} = 5.3$ V, $\mathrm{Vdd} = 6.1$ V, and $\mathrm{Vdd} = 6.9$ V.

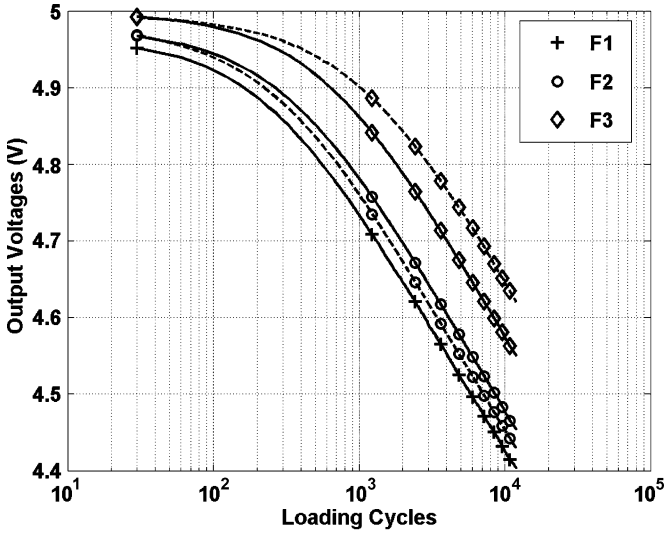

(a)

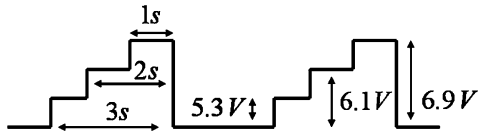

(b)

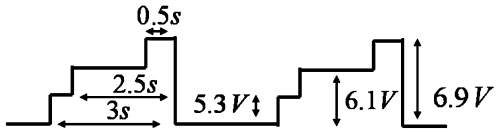

(c)

Fig. 12. (a) Voltage measured at the output of each injector when the sensor is subjected to periodic cycles shown in (b) and (c), each of which simulates the signal generated by the piezoelectric transducer.

cycles, the transducer can easily generate voltage levels close to 7 V. The measured response for each of the injectors in the array is shown in Fig. 13(b). The results clearly show the monotonic response across the three injectors and that each response is proportional to the total duration for which the strain levels exceeded the programmed thresholds. The injector responses were then calibrated against Fig. 11 and (10) to determine the loading statistics which can then be used in Miner's rule. For instance, the cumulative loading statistics calculated at a given time are indicated on Fig. 13(b), which shows that 30% of the time the structure experienced strain levels exceeding the threshold for injector 1, 16% of the time experienced strain levels exceeding the threshold for injector 2, and less than 1% of the time experienced strain levels exceeding the threshold for injector 3.

The power dissipation of the sensor (current reference and floating gate array) was calculated at different voltage levels and is summarized in Fig. 14. It can be seen that the total current drawn by the sensor saturates around 6.5 V, where all of the injectors become active. Thus, the nominal power dissipation of the sensor at 5.5 V is 800 nW. More importantly, the impedance of the sensor is 40 Mω, implying that the proposed sensor could also be interfaced with other power-harvesting sources that typically have low current driving capability.

VI. Discussions and Conclusion

In this paper, we presented a novel piezo-powered floating gate sensor array that can sense, compute, and store cumulative

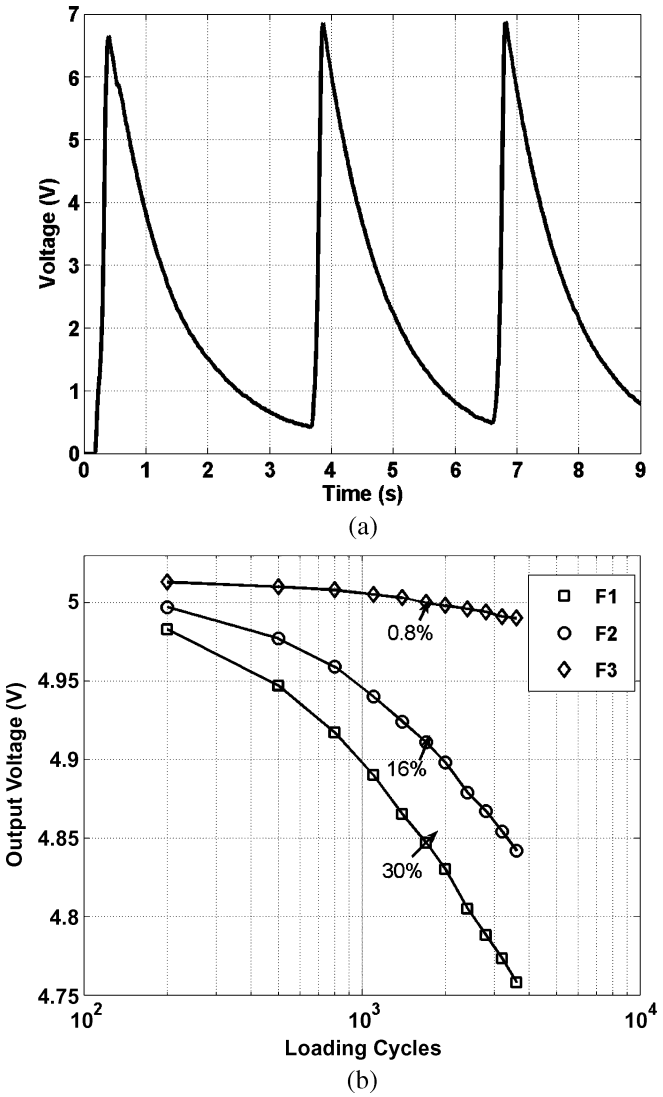

Fig. 13. (a) Voltage generated by a PZT in response to periodic loading. (b) Measured response of the floating-gate injector array.

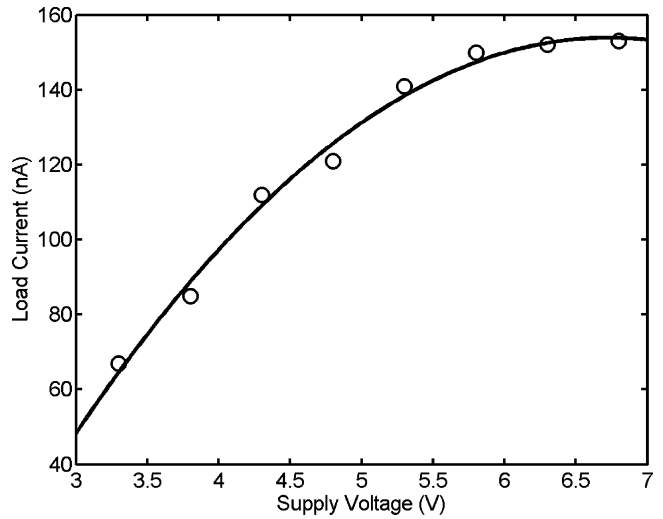

Fig. 14. Supply current drawn by the sensor at different supply voltages.

statistics of loading cycles experienced by a mechanical structure. The nominal power dissipation of the integrated circuit is less than 1 μW, which along with its small form factor makes it ideal for embedded sensing in biomechanical implants. One of the key challenges in deploying the sensor *in-vivo* will be remote access to the loading statistics accumulated on the floating-gate sensor. Our long-term goal of this research is to interface the sensor array to a data transmission module that can be remotely powered and interrogated using inductive coupling.

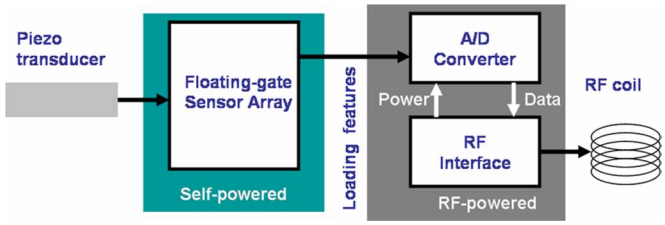

Fig. 15. System architecture of a complete implanted device that integrates the proposed floating-gate sensor array.

Fig. 15 shows a system-level architecture of a complete implanted sensor that employs the proposed piezo-floating-gate array. The sensor will consist of two subsystems: 1) a self-powered subsystem consisting of a floating-gate sensor array and 2) a radio-frequency identification (RFID) interface that facilitates remote access to the stored features. Before the sensor is deployed, the floating-gate array is calibrated/equalized offline using the algorithm described in Fig. 10. The operation of a deployed sensor will then consist of two modes: 1) continuous monitoring mode, where the energy harvested from the applied mechanical stresses is used for computing and storing loading statistics and 2) access mode, where an RF reader is brought in proximity to the sensor (for example during scheduled checkup) which powers up the analog-to-digital converters and transfers the digitized representation of the stored statistics to a reader over the RF link. A medical practitioner can then calibrate the measured statistics with a known response of the PZT to determine the remaining life of the implant.

Even though the paper discusses only biomedical applications of the floating-gate sensor, the device could be used in other autonomous sensing applications that range from infrastructure monitoring in civil engineering applications to usage monitoring in military applications.

REFERENCES

[1] S. Kurtz, K. Ong, E. Lau, F. Mowat, and M. Halpern, "Projections of primary and revision hip and knee arthroplasty in the United States from 2005 to 2030," *J. Bone Joint Surg.*, vol. 89, no. 4, pp. 780–785, 2007.

[2] M. A. McGee, D. W. Howie, K. Costi, D. R. Haynes, C. I. Wildenauer, M. J. Pearcy, and J. D. McLean, "Implant retrieval studies of the wear and loosening of prosthetic joints: A review," *Wear*, vol. 241, no. 2, pp. 158–165(8), July 31, 2000.

[3] P. F. Sharkey, W. J. Hozack, R. H. Rothman, S. Shastri, and S. M. Jacoby, "Why are total knee arthroplasties failing today?," *Clin. Orthopaed. Related Res.*, vol. 404, pp. 7–13, Nov. 2002.

[4] B. A. Morris, D. D. D'Lima, J. Slamin, N. Kovacevic, S. W. Arms, C. P. Townsend, and C. C. Colwell, Jr., "E-Knee: Evolution of the electronic knee prosthesis," *J. Bone Joint Surg. Amer. A*, vol. 83, no. Suppl 2, pt. 1, pp. 62–66, 2001.

[5] S. J. G. Taylor and P. S. Walker, "Forces and moments telemetered from two distal femoral replacements during various activities," *J. Biomech.*, vol. 34, pp. 839–848, 2001.

[6] M. M. Maliniak, J. A. Szivek, D. W. DeYoung, and J. Emmanual, "Hydroxyapatite-coated strain gauges for long-term in vivo bone strain measurements," *J Appl Biomater.*, vol. 4, pp. 143–152, 1993.

[7] D. T. Davy, G. M. Kotzar, R. H. Brown, K. G. S. R. Heiple, V. M. Goldberg, K. G. Heiple, Jr, J. Berilla, and A. H. Burstein, "Telemetric force measurements across the hip after total arthroplasty," *J Bone Joint Surg A*, vol. 70, pp. 45–50, 1988.
[8] N. Elvin, A. Elvin, and D. H. Choi, "A self-powered damage detection sensor," *J. Strain Anal. Eng. Design*, vol. 38, no. 2, pp. 115–125, 2003.
[9] E. Häsler, L. Stein, and G. Harbauer, "Implantable physiological power supply with PVDF film," *Ferroelectrics*, vol. 60, pp. 277–282, 1984.
[10] G. V. B. Cochran, M. W. Johnson, M. P. Kadaba, F. Vosburgh, M. W. Ferguson-Pell, and V. R. Palmeiri, "Piezoelectric internal fixation devices: A new approach to electrical augmentation of osteogenesis," *J. Orthopaed. Res.*, vol. 3, no. 4, pp. 508–513.
[11] N. Elvin, A. Elvin, and M. Spector, "Smart Orthopaedic Implant," U.S. Patent 6 034 296, Mar. 7, 2000.
[12] S. R. Platt, S. Farritor, K. Garvin, and H. Haider, "The use of piezoelectric ceramics for electric power generation within orthopedic implants," *IEEE/ASME Trans. Mech.*, vol. 10, no. 4, pp. 455–461, Dec. 2005.
[13] J. B. Park, A. F. von Recum, G. H. Kenner, B. J. Kelly, W. W. Coffeen, and M. F. Grether, "Piezoelectric ceramic implants: A feasibility study," *J. Biomed. Mater. Res.*, vol. 14, no. 3, pp. 269–277, 1980.
[14] N. Mukherjee, R. D. Roseman, and J. P. Willging, "The piezoelectric cochlear implant: Concept, feasibility, challenges, and issues," *J. Biomed. Mater. Res.*, vol. 53, no. 2, pp. 181–187.
[15] J. Snoeck, M. Berkhof, M. Claeys, C. Vrints, J. Bosmans, H. Decoster, and H. Heuten, "External vibration interference of activity based rate responsive pacemakers," *Pacing Clin. Electrophysiol.*, vol. 15, no. 11, pp. 1841–1845, 1992.
[16] W. B. Phillips, B. C. Towe, and P. J. Larson, "An ultrasonically-driven piezoelectric neural stimulator," in *Proc. 25th Annu. Int. Conf. IEEE EMBS Soc.*, 2003, pp. 1983–1986.
[17] C. C. Enger and J. H. Kennedy, "An improved bioelectric generator," *Trans. Amer. Soc. Artif. Intern. Organs*, vol. 10, pp. 373–377, Oct. 1964.
[18] S. W. Arms, C. P. Townsend, D. L. Churchill, and N. Phan, "Energy harvesting, wireless, strain sensor for damage tracking of helicopter components," presented at the 3rd Eur. Workshop Structural Health Monitoring, Jul. 5–7, 2006.
[19] T. Wright, F. Glowczewski, D. Cowin, and D. Wheeler, "Ulnar nerve excursion and strain at the elbow and wrist associated with upper extremity motion," *J. Hand Surg. Amer.*, vol. 26, no. 4, pp. 655–662, July 2001.
[20] J. Borodkin, N. Caldwell, and S. Hollister, "The influence of mechanical strain magnitude on bone adaptation to porous coated implants," in *Proc. IEEE Eng. Med. Biol. Soc. Conf.*, 1999, p. 768.
[21] B. D. Beynnon and B. C. Fleming, "Anterior cruciate ligament strain in-vivo: A review of previous work," *J. Biomech.*, vol. 31, pp. 519–525, 1998.
[22] R. L. Pradhan, E. Itoi, Y. Hatakeyama, M. Urayama, and K. Sato, "Superior labral strain during the throwing motion: A cadaveric study," *Amer. J. Sports Med.*, vol. 29, pp. 488–492, 2001.
[23] N. Lajnef, S. Chakrabartty, N. Elvin, and A. Elvin, "Piezo-powered floating gate injector for self-powered fatigue monitoring in biomechanical implants," in *Proc. IEEE Symp. Circuits Syst. (ISCAS'2007)*, New Orleans, LA, 2007, pp. 88–92.
[24] S. Suresh, *Fatigue of Materials*, 2nd ed. Cambridge, U.K.: Cambridge Univ. Press, 1998.
[25] S. S. Mason, "Fatigue—A complex subject," *Exper. Mech.*, vol. 5, no. 7, pp. 193–226, 1965.
[26] C. Dorio, P. Hasler, B. Minch, and C. A. Mead, "A single-transistor silicon synapse," *IEEE Trans. Electron Devices*, vol. 43, no. 11, pp. 1972–1980, Nov. 1996.

Nizar Lajnef (S'05) received the degree in mechanical engineering and the M.S. degree in computational mechanics from Tunisia Polytechnic School (TPS), Tunis, Tunisia, in 2004 and 2005, respectively, and the M.S and Ph.D. degrees in civil engineering from Michigan State University (MSU), East Lansing, in 2008.

He performed research with the Adaptive Integrated Microsystems Laboratory Group, Department of Electrical and Computer Engineering, MSU. He is currently an Assistant Professor with MSU.

Niell G. Elvin received the B.Sc. degree from the University of the Witwatersrand, South Africa, in 1994 and the S.M. and Ph.D. degrees from the Massachusetts Institute of Technology (MIT), Cambridge, in 1995 and 1998, respectively.

He is currently a Research Scientist with Columbia University, New York, NY. Before joining Columbia University, he was an Assistant Professor with Michigan State University, East Lansing. His research interests include smart material systems, sensors, and instrumentation.

Shantanu Chakrabartty (M'96) received the B.Tech degree from the Indian Institute of Technology, Delhi, in 1996, and the M.S and Ph.D. degrees in electrical engineering from Johns Hopkins University, Baltimore, MD, in 2001 and 2004 respectively.

He is currently an Assistant Professor with the Department of Electrical and Computer Engineering, Michigan State University, East Lansin. From 1996 to 1999, he was with Qualcomm Inc., San Diego, CA, and, during 2002, he was a Visiting Researcher with the University of Tokyo, Tokyo, Japan. His current research interests include low-power analog and digital VLSI systems and hardware implementation of machine learning algorithms with application to biosensors and biomedical instrumentation.

Dr. Chakrabartty was a recipient of The Catalyst Foundation Fellowship from 1999 to 2004 and the Best Undergraduate Thesis Award in 1996. He is currently a member of the IEEE BioCAS technical committee and the IEEE Circuits and Systems Sensors technical committee and serves as an Associate Editor for *Advances in Artificial Neural Systems*.